

Novel quasi-2D metal in CuSe-based layered compound: $\text{Bi}_2\text{YO}_4\text{Cu}_2\text{Se}_2$

S. G. Tan,^{†,§} D. F. Shao,^{†,§} W. J. Lu,[†] W. H. Song,[†] Hechang Lei,^{*,†} and Y. P. Sun^{*,†,‡,¶}

Key Laboratory of Materials Physics, Institute of Solid State Physics, Chinese Academy of Sciences, Hefei 230031, People's Republic of China, High Magnetic Field Laboratory, Chinese Academy of Sciences, Hefei 230031, People's Republic of China, and University of Science and Technoly of China, Hefei 230026, People's Republic of China

E-mail: hchlei@issp.ac.cn; ypsun@issp.ac.cn

Abstract

We have investigated the physical properties of a new layered oxyselenide $\text{Bi}_2\text{YO}_4\text{Cu}_2\text{Se}_2$, which crystallizes in an unusual intergrowth structure with Cu_2Se_2 and Bi_2YO_4 layers. Electric transport measurement indicates that $\text{Bi}_2\text{YO}_4\text{Cu}_2\text{Se}_2$ behaves metallic. Thermal transport and Hall measurements show that the type of the carriers is hole-like and it may be a potential thermoelectric material at high temperatures. First principle calculations are in agreement with experimental results and show that $\text{Bi}_2\text{YO}_4\text{Cu}_2\text{Se}_2$ is a quasi-2D metal. Further theoretical investigation suggests that all the CuSe-based compounds with $\text{Bi}_2\text{YO}_4\text{Cu}_2\text{Se}_2$ -type structure should be metallic, which is very unique in the known CuSe-based compounds.

*To whom correspondence should be addressed

[†]Key Laboratory of Materials Physics, Institute of Solid State Physics, Chinese Academy of Sciences

[‡]High Magnetic Field Laboratory, Chinese Academy of Sciences

[¶]University of Science and Technoly of China

[§]The authors contributed equally to this work.

INTRODUCTION

Quasi-two-dimensional (quasi-2D) oxide compounds of transition-metal elements have been studied extensively because of their exotic and superior electrical and magnetic properties, such as high-temperature superconducting cuprates,¹ manganites with colossal magnetoresistance,² and cobaltite-based thermoelectric materials,³ etc.. In contrast, oxychalcogenides, which also tend to adopt layered structure due to the different sizes and coordination requirements of oxygen and the heavier chalcogenide anions, are a relatively under-investigated class of solid-state compounds.⁴ Among known layered TMCh-based (TM = Cu, Ag; Ch = S, Se, Te) oxychalcogenides, there are mainly two structural types summarized by Clarke.⁴ One structural type is representative by the LnOTMCh series (Ln = lanthanide), which can be regarded as the filled PbFCl-type structure and is isostructural to ZrSiCuAs as well as iron-based superconductors LnOFePn (Pn = As, P).^{5,6} These compounds are composed of alternating Ln₂O₂ fluorite layers and TM₂Ch₂ antifluorite layers along *c* axis and have been studied intensively because of their superior and novel optical and transport properties originating from TM₂Ch₂ layers.⁷⁻¹⁰ Another important structural type is that first described for the oxide antimonide Sr₂Mn₃Sb₂O₂¹¹ (which may conveniently be formulated as Sr₂MnO₂Mn₂Sb₂) and related oxide pnictides.^{12,13} Later on, this structural type is also found in Sr₂ZnO₂Cu₂S₂.¹⁴ In Sr₂ZnO₂Cu₂S₂, the chalcogenide layer [Cu₂S₂]²⁻ is similar to that in LaO-CuS whereas the [Sr₂ZnO₂]²⁺ is not fluorite type but perovskite type. Several oxychalcogenides with this crystal structure have been reported.¹⁴⁻¹⁹

As listed in Table 1, most of the reported CuCh-based layered compounds are semiconductors.^{19,21-23,26,27} But it is well-established²⁸ that the copper chalcogenide layers present in the oxy-sulfides can readily accept holes in the antibonding states at the top of a valence band that is composed of well-mixed Cu-3*d* and S-3*p* orbitals, and these holes are very mobile. For example, La_{1-x}Sr_xOCuS is a rare example of a transparent *p*-type semiconductor²⁹ in which the Cu-3*d*/S-3*p* valence band is doped with holes; the band gap insulator Sr₂ZnO₂Cu₂S₂ can also be doped to produce a metallic Na_xSr_{2-x}ZnO₂Cu₂S₂ with *p*-type carriers with *x* ~ 0.1,³⁰ and there is evidence for the very high mobility of *p*-type carriers in the related Sr₃Sc₂O₅Cu₂S₂ with Cu or Sr defi-

Table 1: Some typical CuCh-based compounds and their ground states.

Compound	Ground state
KCu ₂ Se ₂	Metallic ²⁰
BaCu ₂ Se ₂	Semiconducting ²¹
LaOCuS(Se)	Semiconducting ²²
BaFCuS(Se)	Semiconducting ²³
BiOCuS(Se)	Semiconducting ²²
YOCuSe	Semiconducting ²⁴
HgOCuSe	Metallic ²⁵
Sr ₂ MnO ₂ Cu ₂ Se ₂	Semiconducting ¹⁹
Sr ₃ Sc ₂ O ₅ Cu ₂ S ₂	Semiconducting ^{26,27}
Bi ₂ YO ₄ Cu ₂ Se ₂	Metallic

ciencies.^{26,27} On the other hand, HgOCuSe²⁵ isostructural to LaOCuS is a metal and KCu₂Se₂²⁰ in which La₂O₂ layer is replaced by alkali metal K also exhibit metallic behavior. Therefore, the physical properties of CuCh-based layered oxychalcogenides are not only determined by the intralayer interaction of CuCh layer alone but also by the interlayer interactions.

Recently, a new series of layered oxychalcogenides Bi₂LnO₄Cu₂Se₂ (Y, Gd, Sm, Nd, and La) were synthesized.³¹ The metallic behavior is stated for the compound Bi₂YO₄Cu₂Se₂ which is very rare in the CuCh-based oxychalcogenides. In this work, we systematically studied the electric transport, heat capacity, thermoelectric properties and the electronic structure of the layered oxy-selenide Bi₂YO₄Cu₂Se₂. Both the results of experiment and theoretical calculation indicate the quasi-2D metallic ground state in this compound. We also found it may be a potential thermoelectric material at high temperatures. Furthermore, we systematically studied the doping effects of such system in theory. The results suggest that the ground state of all the CuSe-based compounds with Bi₂YO₄Cu₂Se₂-type structure should be metallic. Such property is very unique in the known CuSe-based compounds, most of which are semiconductors.

EXPERIMENT SECTION

Synthesis.

$\text{Bi}_2\text{YO}_4\text{Cu}_2\text{Se}_2$ sample was prepared by reacting a stoichiometric mixture of Bi_2O_3 , Y_2O_3 , Y, Cu, and Se. The raw materials were mixed and ground thoroughly in an agate pestle and mortar, and then the mixtures were pressed into pellets under 12 MPa. The pellets were placed into dried alumina crucibles and sealed under vacuum ($< 10^{-4}$ Pa) in the silica tubes which had been baked in drybox for 1-2 h at 150°C . The ampoules were heated to 830°C with $1^\circ\text{C}/\text{min}$ and maintained at this temperature for 24 h. Finally the furnace is shut down and cools to room temperature naturally. The obtained samples were reground, pelletized, and heated for another 24 hours at 830°C followed by furnace cooling.

Structure and Composition Analysis.

The X-ray powder diffraction patterns were recorded at room temperature on a Panalytical diffractometer (X'Pert PRO MRD) with $\text{Cu-K}\alpha$ radiation (40 kV, 40 mA) and a graphite monochromator in a reflection mode ($2\theta = 10 - 80^\circ$, step = 0.016° , scan speed = 5 s/step). Well grounded fine powder samples on glass slides were used to collect the diffraction pattern. Structural refinement of powder $\text{Bi}_2\text{YO}_4\text{Cu}_2\text{Se}_2$ sample was carried out by using Rietica software.³² The average stoichiometry of a $\text{Bi}_2\text{YO}_4\text{Cu}_2\text{Se}_2$ polycrystalline was determined by examination of multiple points using an energy-dispersive X-ray spectroscopy (EDX) in a JEOL JSM-6500 scanning electron microscope.

X-ray Photoelectron Spectroscopy (XPS).

The XPS data were taken on an AXIS-Ultra instrument from Kratos using monochromatic Al $\text{K}\alpha$ radiation (225 W, 15 mA, 15 kV) and low-energy electron flooding for charge compensation. To compensate for surface charges effects, binding energies were calibrated using the C-1s hydrocar-

bon peak at 284.80 eV. The XPS data were converted into the VAMAS file format and imported into the CasaXPS software package for manipulation and curve-fitting.

Measurement of Electronic Properties.

The electrical resistivity and specific heat were measured using a Quantum Design Physical Properties Measurement System (PPMS) from 300 K to 2 K. Hall measurements were performed from 300 K to 25 K in the PPMS chamber using a Keithley 6220 current source and a Keithley 2182A nanovoltmeter. The Hall coefficient was obtained from the linear fit of the Hall resistivity versus magnetic field between -5 T and 5 T. Seebeck coefficient was measured on bars cut from the pellets. The measurements were performed by the differential method with two T-type thermocouples by using the slope of V - T curve with gradients up to about 0.2 K/mm, by using a laboratory made system in a He-free cryostat.

Density Functional Theory Calculations.

Electronic structure was obtained from first-principles density functional theory (DFT) in the generalized gradient approximation (GGA) according to the Perdew-Burke-Ernzerhof.³³ The QUANTUM-ESPRESSO package³⁴ was used with ultrasoft pseudopotential from GBRV pseudopotential library.³⁵ The discussion about the Coulomb correlation of $3d$ electrons in $\text{Bi}_2\text{YO}_4\text{Cu}_2\text{Se}_2$ was carried out using the GGA+ U approach in the version introduced by Anisimov et al.³⁶ with an approximate self-interaction correction implemented in the rotationally invariant way according to Liechtenstein et al.³⁷ We tested different values of the screened Coulomb parameter U . The exchange parameter J was fixed to $\sim 0.1U$. The energy cutoff for the plane-wave basis set was 40 Ry. Brillouin zone sampling is performed on the Monkhorst-Pack (MP) mesh³⁸ of $16 \times 16 \times 8$.

RESULTS AND DISCUSSION

Crystal Structure, Composition, and Valence State.

The structure of $\text{Bi}_2\text{YO}_4\text{Cu}_2\text{Se}_2$ is shown in Figure 1, which can be described as stacking of edge-shared CuSe_4 tetrahedron layers with Bi_2YO_4 layers alternatively along c axis. Figure 2 (a) shows

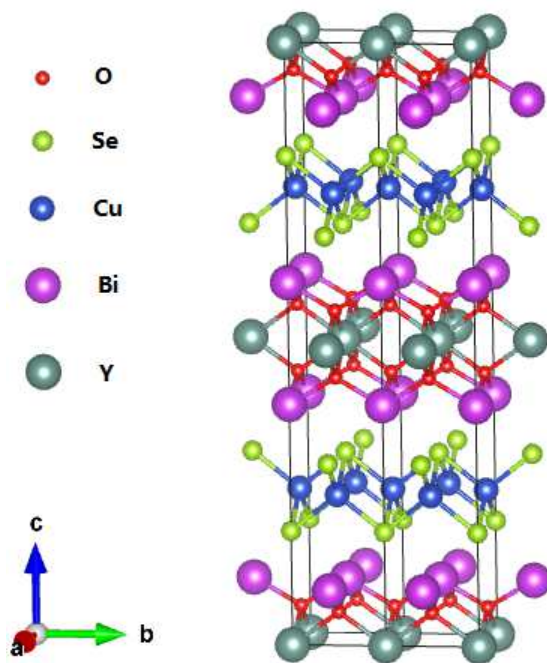


Figure 1: The crystal structure of $\text{Bi}_2\text{YO}_4\text{Cu}_2\text{Se}_2$.

the XRD pattern and the result of Rietveld refinement. The structural parameters obtained from the Rietveld refinements are listed in Tables 2 and 3. Almost all the reflections can be indexed in the space group of $I4/mmm$. The refined lattice parameters of $\text{Bi}_2\text{YO}_4\text{Cu}_2\text{Se}_2$ are $a = 3.8628(3) \text{ \AA}$ and $c = 24.322(2) \text{ \AA}$, which is consistent with the previous reported results for $\text{Bi}_2\text{YO}_4\text{Cu}_2\text{Se}_2$.³¹ The other weak reflections originate from the BiOCuSe impurity, and the result of the two-phase fitting reveals that the weight percentage of BiOCuSe is about 3.24%, which can be neglected to our study on $\text{Bi}_2\text{YO}_4\text{Cu}_2\text{Se}_2$. The EDX spectrum (Figure 2 (b)) of polycrystal confirms the presence of Bi, Y, O, Cu, and Se. The average atomic ratios determined from EDX are Bi: Y: Cu: Se = 1.99(4) : 1.00(2) : 1.99(1) : 1.81(5) when setting the content of Y as 1. It is consistent with the formula $\text{Bi}_2\text{YO}_4\text{Cu}_2\text{Se}_2$. In order to determine the valence state of Cu, Bi, and Y, the

XPS spectrum was measured for the $\text{Bi}_2\text{YO}_4\text{Cu}_2\text{Se}_2$. From Figure 2 (c), it can be seen four peaks located at binding energies (BE) of 163.6, 161.5, 158.4, and 156.4 eV, which can be attributed to $\text{Bi-}4f_{5/2}$, $\text{Y-}3d_{3/2}$, $\text{Bi-}4f_{7/2}$, and $\text{Y-}3d_{5/2}$ respectively, indicating the Bi and Y ions adopt the valence of +3. In Figure 2 (d), the profiles of $\text{Cu-}2p_{3/2}$ and $\text{Cu-}2p_{1/2}$ signals show no obvious multiplet peaks and satellite peaks that are inherent with Cu^{2+} ions, indicating the Cu ions predominately adopt the monovalence state, and the monovalence state of Cu ion is common in other CuCh-based compounds.^{19–24}

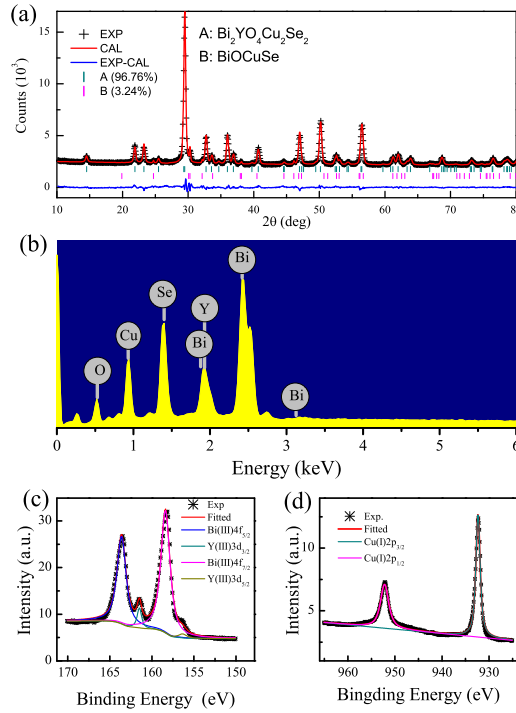


Figure 2: (a) Result of Rietveld refinement against powder XRD diffraction data for $\text{Bi}_2\text{YO}_4\text{Cu}_2\text{Se}_2$; (b) is the EDX spectrum of the sample; (c) and (d) are the XPS spectra of Bi, Y and Cu.

Physical Properties.

As shown in Figure 3, the resistivity $\rho(T)$ of polycrystalline $\text{Bi}_2\text{YO}_4\text{Cu}_2\text{Se}_2$ shows a metallic behavior in the measured temperature region. The resistance drops linearly with temperature from 300 to 100 K and the room temperature value of resistivity is $0.59 \text{ m}\Omega \cdot \text{cm}$, which is much smaller than the reported value.³¹ The temperature coefficient of resistivity is $1.7 \times 10^{-3} \text{ m}\Omega \cdot \text{cm}/\text{K}$. It

should be noted that the polycrystalline BiOCuSe shows semiconducting behavior. The impurity may have some minor influence on the absolute value of resistivity, but the metallic behavior should be intrinsic. As can be seen, below 45 K the resistivity is satisfied with the equation

$$\rho(T) = \rho_0 + AT^2, \quad (1)$$

which is suggestive of Fermi liquid behavior in the ground state. The residual resistivity ρ_0 and parameter A are found to be $134.7(3) \mu\Omega \cdot \text{cm}$ and $0.01118(3) \mu\Omega \cdot \text{cm}/\text{K}^2$ respectively. The metallic behavior is consistent with our theoretical calculation results as shown below.

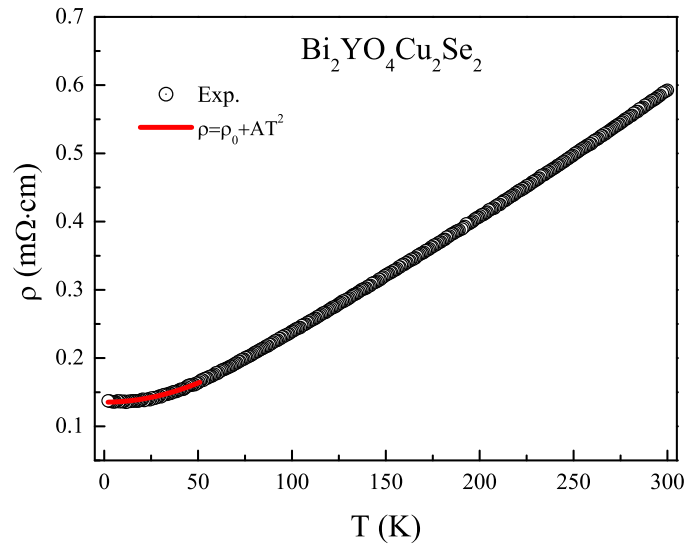


Figure 3: Electrical resistivity of $\text{Bi}_2\text{YO}_4\text{Cu}_2\text{Se}_2$ is plotted as a function of temperature from 300 to 2 K, and the red line is the Fermi liquid fitting of the resistivity at low temperature.

On the other hand, previous theoretical reports have indicated that the undoped BiOCuSe is a semiconductor and the metallic behavior of BiOCuSe is caused by Cu deficiencies which introduce holes to the system.^{22,39} In undoped BiOCuSe, the “electricity storage” layer Bi_2O_2 provides two electrons to the “conductive” layer Cu_2Se_2 . However, in $\text{Bi}_2\text{YO}_4\text{Cu}_2\text{Se}_2$, the “electricity storage” layer Bi_2YO_4 provides only one electron to the “conductive” layer Cu_2Se_2 . Therefore, the replacement of Bi_2O_2 by Bi_2YO_4 should introduce holes and as a result, $\text{Bi}_2\text{YO}_4\text{Cu}_2\text{Se}_2$ is a metal with p -type carriers. There will be further discussion in the calculation part. Figure 4 shows the

Table 2: Fractional atomic coordinates of $\text{Bi}_2\text{YO}_4\text{Cu}_2\text{Se}_2$ and BiOCuSe determined by two-phase refinement of X-ray data.

Atom	x	y	z
$\text{Bi}_2\text{YO}_4\text{Cu}_2\text{Se}_2$ (wt%: 96.76%)			
Bi	0.5	0.5	0.8968(1)
Y	0.5	0.5	0.5
O	0	0.5	0.9353(7)
Cu	0	0.5	0.25
Se	0.5	0.5	0.3110(2)
BiOCuSe (wt%: 3.24%)			
Bi	0.25	0.25	0.141(2)
Cu	-0.25	0.25	0.5
Se	-0.25	-0.25	0.342(5)
O	-0.25	0.25	0

Table 3: Structural parameters obtained from Rietveld analysis at room temperature.

	$\text{Bi}_2\text{YO}_4\text{Cu}_2\text{Se}_2$	BiOCuSe
space group	I4/mmm	P4/nmm
a (Å)	3.8628(3)	3.9311(7)
c (Å)	24.322(2)	8.899(3)
bond length		
$d_{\text{Bi-O}}$ (Å)	2.399(1)	2.34(3)
$d_{\text{Bi-Se}}$ (Å)	3.437(4)	3.30(1)
$d_{\text{Cu-Se}}$ (Å)	2.435(3)	2.42(2)
bond angle		
O-Bi-O	79.02(3) \times 4 128.27(3) \times 2	73.06(1) \times 4
O-Y-O	66.48(3) \times 4 101.7(4) \times 2	
Se-Cu-Se	104.94(1) \times 2 111.78(1) \times 4	108.75(1) \times 2 109.84(2) \times 4

specific heat of $\text{Bi}_2\text{YO}_4\text{Cu}_2\text{Se}_2$ measured from 280 K to 5 K. The specific heat of $\text{Bi}_2\text{YO}_4\text{Cu}_2\text{Se}_2$ approaches to the value of $3NR$ at 280 K, where N is the atomic number in the chemical formula ($N = 11$) and R is the gas constant ($R = 8.314 \text{ J/mol}\cdot\text{K}$), consistent with the Dulong-Petit law. The

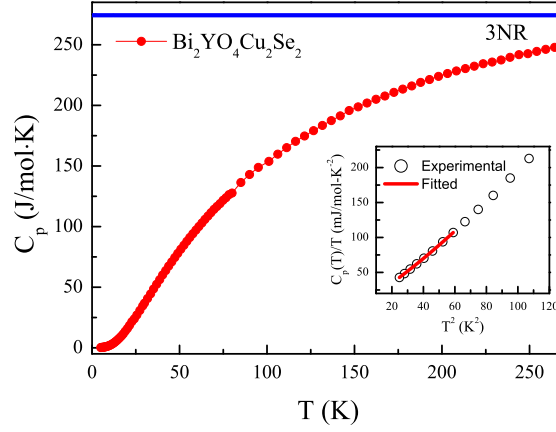


Figure 4: Temperature dependence of specific heat for $\text{Bi}_2\text{YO}_4\text{Cu}_2\text{Se}_2$. The inset is the low temperature data $C_p(T)/T$ plotted as a function of T^2 .

inset shows the low-temperature specific heat data, $C_p(T)/T$ plotted as a function of T^2 . It can be fitted using

$$C_p = \gamma T + \beta T^3 + \delta T^5, \quad (2)$$

where γT is the electronic contribution with γ the Sommerfeld coefficient, and $\beta T^3 + \delta T^5$, originate from the lattice contribution. The fitted values of γ , β , and δ are equal to $3.6(8) \text{ mJ/mol}\cdot\text{K}$, $1.56(3) \text{ mJ/mol}\cdot\text{K}^4$, and $0.0038(3) \text{ mJ/mol}\cdot\text{K}^6$ respectively. Using the formula

$$\Theta_D = \left(\frac{n \times 1.944 \times 10^6}{\beta} \right)^{1/3}, \quad (3)$$

where n is the number of atoms in a unit cell, we derived the Debye temperature $\Theta_D = 239 \text{ K}$. According to the Sommerfeld theory of metals, γ can be written as function of the density of states (DOS) at Fermi level as:

$$\gamma = \frac{\pi^2 k_B^2}{3} N(E_F) (1 + \lambda), \quad (4)$$

where $N(E_F)$ is the DOS at the Fermi level and λ is the electron-phonon coupling constant. As-

suming λ is 0, the obtained value of $N(E_F)$ is 1.5 states/eV/f. u..

The thermal transport measurement results including the Seebeck coefficient S , electrical conductivity σ , and thermal conductivity κ are shown in Figure 5. The S is positive in the whole measurement temperature region, indicating the major carriers are holes. The $S(T)$ is nearly linearly dependent with temperature and drops to zero at low temperature. The $\kappa(T)$ is almost constant when T is above 100 K, below which the $\kappa(T)$ drops fast near to zero. The dimensionless figure of merit, ZT ($ZT = S^2T\sigma/\kappa$), which represents for the efficiency of a thermoelectric material, was calculated and presented in Figure 5 (d). Due to the low resistivity, and relatively small thermal conductivity, the ZT value of our sample at 300 K reaches about 0.012. And the value of ZT increases smoothly from 5 K to 300 K. It implies $\text{Bi}_2\text{YO}_4\text{Cu}_2\text{Se}_2$ may be a potential thermoelectric material at high temperatures.

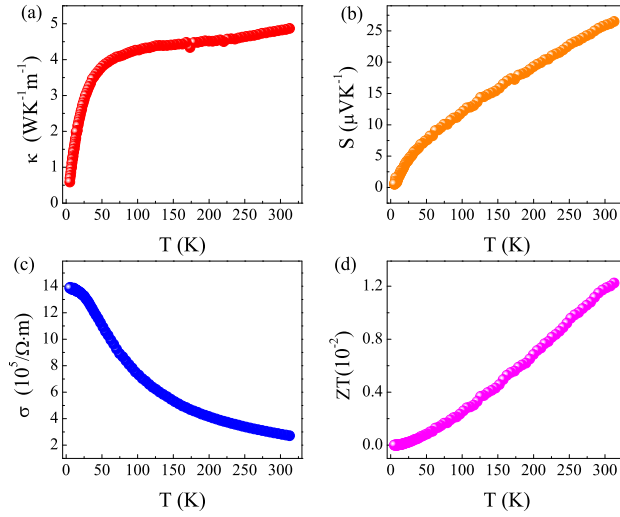


Figure 5: (a) The thermal conductivity κ , (b) Seebeck coefficient S , (c) electrical conductivity σ and (d) figure of merit ZT as a function of temperature from 330 to 5 K.

In order to confirm the type of carrier and determine the carrier density in $\text{Bi}_2\text{YO}_4\text{Cu}_2\text{Se}_2$, the magnetic field dependence of the Hall resistivity at various temperatures is shown in Figure 6. The transverse resistivity $\rho_{xy}(H)$ shows an approximately linear relation against the magnetic field and is positive at all measuring temperatures, indicating that the hole-type carrier is dominant, consistent with the sign of $S(T)$. From the linear fitting of $\rho_{xy}(H) - H$ relation, we obtain the Hall coefficient $R_H = \rho_{xy}(H)/H$ at different temperatures, which is shown in Figure 6 (b). It can be

seen that R_H decreases with temperature. The change can be ascribed to the multiband effect, which has been observed in classic two-band superconducting materials such as MgB_2 ⁴⁰ as well as in iron based material $\text{Nd}(\text{O},\text{F})\text{FeAs}$.⁴¹ A multiband electronic structure at the Fermi level is also supported by the DFT calculations discussed below.

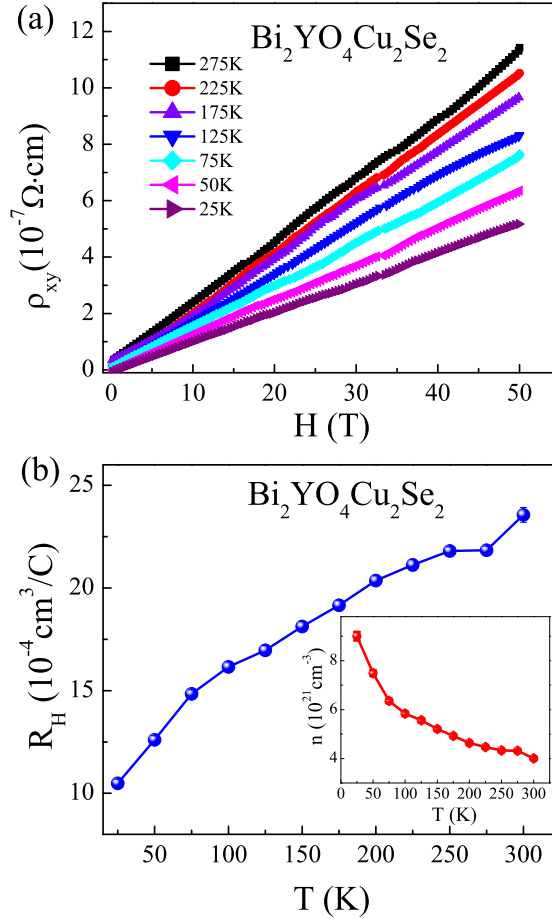


Figure 6: (a) Field dependence of $\rho_{xy}(H)$ at various temperatures. (b) Temperature dependence of the Hall coefficient R_H of $\text{Bi}_2\text{YO}_4\text{Cu}_2\text{Se}_2$. Inset: temperature dependence of the carrier density $n=1/|eR_H|$ calculated from R_H .

Electronic Structure of $\text{Bi}_2\text{YO}_4\text{Cu}_2\text{Se}_2$.

The crystal structure of $\text{Bi}_2\text{YO}_4\text{Cu}_2\text{Se}_2$ was optimized with respect to lattice parameters and atomic positions. The optimized lattice parameters and atomic coordinates are listed in Table 4. The structure is in good agreement with experimental observation except for the slight overestimation

of c (2.3% relative to experimental value), which is expected within the GGA.

Table 4: The optimized lattice parameters and atomic coordinates compared with experimental values.

	Exp.	Opt.
a (Å)	3.8628(3)	3.888
c (Å)	24.322(2)	24.872
$z(\text{Bi})$	0.8968(1)	0.89895
$z(\text{Y})$	0.5	0.5
$z(\text{O})$	0.9353(7)	0.94445
$z(\text{Cu})$	0.25	0.25
$z(\text{Se})$	0.3110(2)	0.31106

The metallic ground state found in experiment is reproduced in our calculation. Figure 7 shows the calculated DOS of $\text{Bi}_2\text{YO}_4\text{Cu}_2\text{Se}_2$. In the valence band, Bi-6 p electrons hybridize with O-2 p electrons in the energy range between -6 eV and -1 eV, and the hybridization of Cu-3 d and Se-4 p electrons is from -6 eV to 0.5 eV across Fermi level (E_F). The conduction bands at high energies, mainly built up of Bi-6 p and O-2 p electrons, are separated by a small gap of ~ 0.25 eV. The E_F locates at a small valley of DOS, leading to the small $N(E_F)$. The calculated $N(E_F)$ (2.1

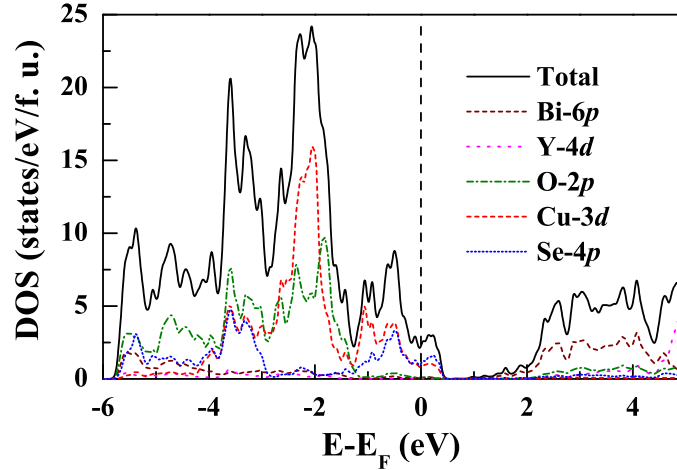


Figure 7: The calculated DOS of $\text{Bi}_2\text{YO}_4\text{Cu}_2\text{Se}_2$.

states/eV/f. u.) is close to the experimental one (1.5 states/eV/f. u.). Figure 8 (a) shows the band structure of $\text{Bi}_2\text{YO}_4\text{Cu}_2\text{Se}_2$. In the k_z direction (perpendicular to the layers), the bands are rarely dispersive. On the other hand, the strong hybridizations between Cu and Se give rise to a strongly

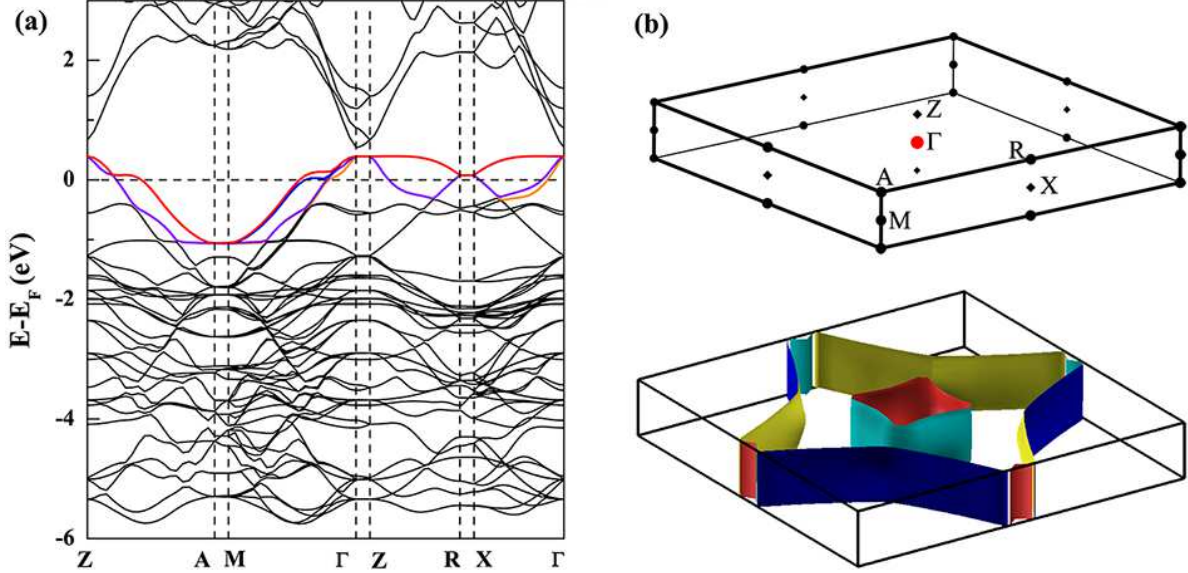


Figure 8: (a) The band structure of $\text{Bi}_2\text{YO}_4\text{Cu}_2\text{Se}_2$. (b) The Brillouin zone and Fermi surface of $\text{Bi}_2\text{YO}_4\text{Cu}_2\text{Se}_2$. In calculations the conventional tetragonal cell (two formulas in a cell) was used.

dispersive band structure in the k_x and k_y (layer-parallel) directions. Similar quasi-2D properties are found in alkali metal intercalated compound KCu_2Se_2 , which also behaves metallic.²⁰ There are four bands (in conventional unit cell) crossing E_F , proving the multiband property and p -type conduction observed by the Hall and thermal transport measurements. Figure 8 (b) shows the obtained 2D hole-type Fermi surface: The lower two bands crossing E_F form two cylinder-type Fermi surface around Γ -Z and X-R; the upper two bands form large Fermi sheet between Γ -Z and M-A. In order to analyze the orbital characters, the “fat-band” of $\text{Bi}_2\text{YO}_4\text{Cu}_2\text{Se}_2$ is also presented (Figure 9). Obviously, the Fermi surface is formed by the bands with prominent hybridization between $d_{xy} + d_{yz}$ of Cu and $p_x + p_y$ of Se. The Se- p_z orbital has almost no contribution at E_F , indicating the absence of conduction between the layers. Such quasi-2D electronic properties of $\text{Bi}_2\text{YO}_4\text{Cu}_2\text{Se}_2$ needs to be further confirmed by experimental studies on the single crystal.

We also performed a GGA+ U calculation considering the strong Coulomb correlation of $3d$ electrons in $\text{Bi}_2\text{YO}_4\text{Cu}_2\text{Se}_2$. The corresponding DOS are presented in Figure 10. It can be found that the Coulomb interactions moves the weight of $3d$ electrons towards lower energy. Such properties have been reported in some NiSe-based superconductors.⁴² Under different U , the $d_{xy} + d_{yz}$ orbitals remain contributing prominently at E_F , which makes the $N(E_F)$ rarely varies. Obviously,

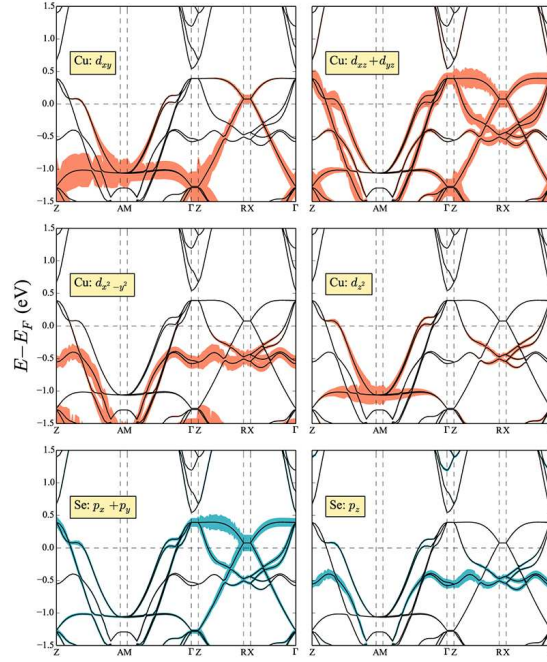


Figure 9: “Fat bands” of $\text{Bi}_2\text{YO}_4\text{Cu}_2\text{Se}_2$, decorated with partial orbital characters of Cu and Se.

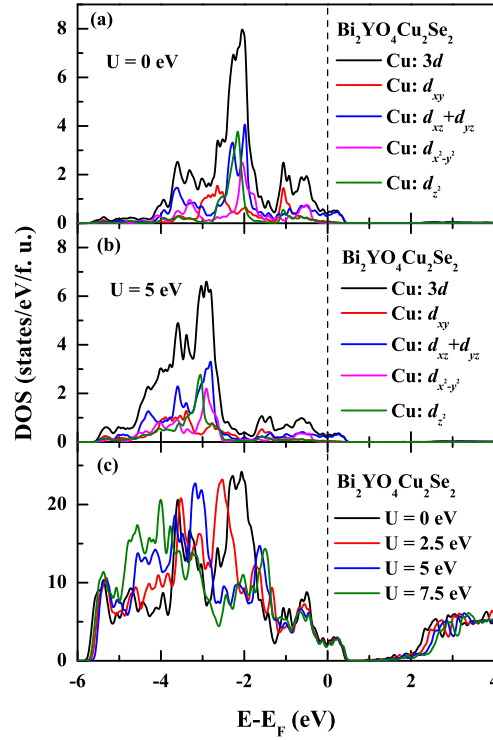


Figure 10: (a) Orbital contribution of DOS of Cu-3d electrons with $U = 0$ eV. (b) Orbital contribution of DOS of Cu-3d electrons with $U = 5$ eV. (c) DOS of $\text{Bi}_2\text{YO}_4\text{Cu}_2\text{Se}_2$ with $U = 0, 2.5, 5,$ and 7.5 eV.

the added Coulomb interactions do not make the system become a Mott insulator. It might be because of the full filled five orbitals of Cu.⁴²

Ground States of $\text{Bi}_2\text{YO}_4\text{Cu}_2\text{Se}_2$ -type Compounds: A DFT Analysis

Based on the calculation above, the metallic ground state of $\text{Bi}_2\text{YO}_4\text{Cu}_2\text{Se}_2$ is verified. However, to the best of our knowledge, most undoped $\text{CuCh}(\text{Ch}=\text{S}, \text{Se})$ -based compounds are semiconductors (see Table 1). The ground states of $\text{Bi}_2\text{YO}_4\text{Cu}_2\text{Se}_2$ -type compounds need to be distinctly clarified. Generally speaking, CuSe -based compounds can be seen as Cu_2Se_2 layer intercalated by some atoms or molecules. Since the valence band maximum (VBM) is mainly composed of the Cu-Se hybridization states, the function of intercalated blocking layers can be simply seen as giving their valence electrons to the bands. In Table 1, it can be found that the ground states are related to the valence states of blocking layers closely: If the valence electrons of the blocking layers are smaller than two, the compounds (e. g., KCu_2Se_2 ,²⁰ HgOCuSe ²⁵) will behave metallic. And all the reported CuSe -based semiconductors have the bivalent blocking layers. We compared the DOS of BiOCuSe , LaOCuSe , $\text{Bi}_2\text{YO}_4\text{Cu}_2\text{Se}_2$, and hypothetical $\text{La}_3\text{O}_4\text{Cu}_2\text{Se}_2$ in Figure 11. For the

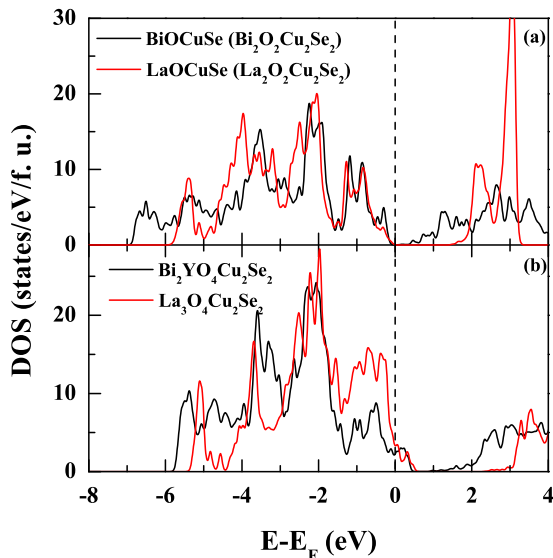


Figure 11: (a) The DOS of BiOCuSe and LaOCuSe . (b) The DOS of $\text{Bi}_2\text{YO}_4\text{Cu}_2\text{Se}_2$, and a hypothetical $\text{La}_3\text{O}_4\text{Cu}_2\text{Se}_2$.

semiconducting BiOCuSe and LaOCuSe, the Bi₂O₂/La₂O₂ blocking layer provides two valence electrons. According to the XPS measurements mentioned above, Bi₂YO₄ layer only gives one valence electrons. Similarly, the La₃O₄ layer should be monovalent. In that case, there is one hole in the valence band, making the systems become metals with *p*-type carriers. Such trend is consistent with the case of ACu₂Se₂ (A is alkali or alkali earth metal).²⁰

If this trend is universal for all the CuSe-based compounds, one may expect that the one electron doping will make Bi₂YO₄Cu₂Se₂/La₃O₄Cu₂Se₂ semiconducting. We calculated the DOS under such doping of Bi₂YO₄Cu₂Se₂ and La₃O₄Cu₂Se₂ using the rigid band approximation (RBA) (Figures 12 (a) and (b)). The results show that the electron doping raises E_F to the gap. In real-

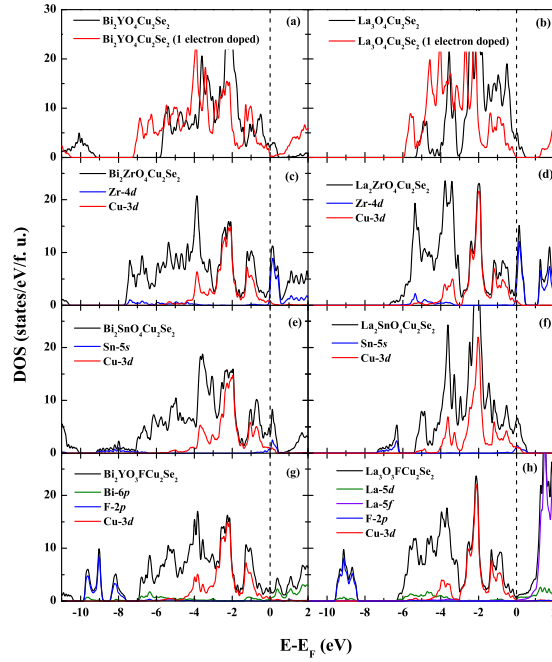


Figure 12: The DOS of one electron doped in Bi₂YO₄Cu₂Se₂ (left panel) and La₃O₄Cu₂Se₂ (right panel). (a) and (b) show the doping effect simulated by simply adding a electron to the system based on RBA. (c)-(h) show the doping effect simulated by doping typical tetravalent cations Zr and Sn or a typical monovalent anion F.

ity, such doping needs to be processed by replacing the trivalent cation Bi/Y/La with a tetravalent cation, or replacing the bivalent anion O with monovalent anions. So we calculated the DOS of Bi₂YO₄Cu₂Se₂ and La₃O₄Cu₂Se₂ with the substitution of the typical tetravalent cations Zr and Sn, and monovalent anion F (Figures 12 (c)-(h)). The results are remarkably different from the calcu-

lation results with RBA. The E_F indeed rises when Y/La is substituted by tetravalent cations. But the substituted cations contribute to the DOS around E_F (Figures 12 (c)-(f)). Thus under such substitutions, the systems are still metallic. On the other hand, when O is substituted by F, E_F moves to the top of Cu-3d band. But the hybridizations between Bi/La and F move the conduction band downwards, which makes the VBM and the conduction band minimum (CBM) partly overlapped. The gap is transformed into a pseudogap. Obviously, the system with a bivalent blocking layer will still be metal. One can further increase the valence electrons by doping more tetravalent cations or monovalent anions to the blocking layer, but the doping effects should be the same. Therefore, it can be deduced that all the CuSe-based compounds with the $\text{Bi}_2\text{YO}_4\text{Cu}_2\text{Se}_2$ -type structure will be metallic. Such structure-related property is very unique in the know CuSe-based compounds.

In fact, the Bi_2YO_4 -type layer can be seen as a stacking of two Bi_2O_2 -type slabs. If we insert more Bi_2O_2 -type slabs into the compounds, we can get a series of compounds with the general formula $[\text{A}_2\text{O}_2(\text{AO}_2)_n]\text{Cu}_2\text{Se}_2$ (A is metal cation). The structure can be viewed as the intercalation of Cu_2Se_2 layer into the $\text{A}_2\text{O}_2(\text{AO}_2)_n$ -type layer inversely. When more A_2O_2 -type slabs are introduced, one can expect that the $\text{A}_2\text{O}_2(\text{AO}_2)_n$ -type layer will play an important role in the transport property together with Cu_2Se_2 layer. In the present case, the bands from the blocking layer can be easily overlapped with the bands from Cu_2Se_2 layer, which makes all the $\text{Bi}_2\text{YO}_4\text{Cu}_2\text{Se}_2$ -type compounds metallic.

Conclusion

In summary, we systematically studied the physical properties of layered oxychalcogenide $\text{Bi}_2\text{YO}_4\text{Cu}_2\text{Se}_2$. It crystallizes in an unusual intergrowth structure with Cu_2Se_2 and Bi_2YO_4 layers. $\text{Bi}_2\text{YO}_4\text{Cu}_2\text{Se}_2$ exhibits metallic behavior with p -type carriers between 2 and 300 K. We obtained a rather large value of ZT at room temperature. Theoretical calculation confirms the quasi-2D metallic behavior of $\text{Bi}_2\text{YO}_4\text{Cu}_2\text{Se}_2$ and indicates the state at Fermi energy originates mainly from Cu-3d and Se-4p electrons.

Based on the comparison of the transport properties of the reported CuSe-based layered compounds, we found that the ground states of the known CuSe-based compounds are related to the valence electrons of their blocking layer: When the number of transferred valence electrons from blocking layer to Cu_2Se_2 layer is smaller than two per layer, the compounds would exhibit metallic behaviors (e. g. KCu_2Se_2 ,²⁰ HgOCuSe ²⁵), but if that number is two, they would become semiconductors. (e. g. BiOCuSe ²²). However, according to our calculations, the present $\text{Bi}_2\text{YO}_4\text{Cu}_2\text{Se}_2$ -type compounds may not obey the rules. The theoretical investigation of doping effects in the system indicates the increase of valence electron of the monovalent blocking layer will change the band structure dramatically and the RBA should be invalid. The Bi_2YO_4 -type blocking layer will play an important role together with Cu_2Se_2 -layer in the transport property, which makes all the $\text{Bi}_2\text{YO}_4\text{Cu}_2\text{Se}_2$ -type compounds metallic. Such property is very unique in the known CuSe-based compounds. The physical properties of other CuSe-based layered compounds need to be studied in the future in order to examine our deduction.

Acknowledgement

This work was supported by the National Key Basic Research under contract No. 2011CBA00111, and the National Nature Science Foundation of China under contract Nos. 51102240, 11104279 and the Joint Funds of the National Nature Science Foundation of China and the Chinese Academy of Sciences Large-scale Scientific Facility (Grant No.U1232139) and Director's Fund of Hefei Institutes of Physical Science, Chinese Academy of Sciences.

References

- (1) Wong-ng, W. K.; Davis, K. L.; Roth, R. S. *J. Am. Ceram. Soc.* **1988**, 71, C64.
- (2) Kimura, T.; Tokura, Y. *Annu. Rev. Mater. Sci.* **2000**, 30, 451.
- (3) Maignan, A.; Hebert, S.; Pi, L.; Pelloquin, D.; Martin, C.; Michel, C.; Hervieu, M.; Raveau, B. *Cryst. Eng.* **2002**, 5, 365.

- (4) Clarke, S. J.; Adamson, P.; Herkelrath, S. J. C.; Rutt, O. J.; Parker, D. R.; Pitcher, M. J.; Smura, C. F. *Inorg. Chem.* **2008**, 47, 8473.
- (5) Kamihara, Y.; Watanabe, T.; Hirano, M.; Hosono, H. *J. Am. Chem. Soc.* **2008**, 130, 3296.
- (6) Kamihara, Y.; Hiramatsu, H.; Hirano, M.; Kawamura, R.; Yanagi, H.; Kamiya T.; Hosono, H. *J. Am. Chem. Soc.* **2006**, 128, 10012.
- (7) Palazzi, M. *Acad. Sci., Paris, C. R.* **1981**, 292, 789.
- (8) Palazzi, M.; Carcaly, C.; Flahaut, J. *J. Solid State Chem.* **1980**, 35, 150.
- (9) Ueda, K.; Inoue, S.; Hirose, S.; Kawazoe, H.; Hosono, H. *Appl. Phys. Lett.* **2000**, 77, 2701.
- (10) Hiramatsu, H.; Kamioka, H.; Ueda, K.; Hirano, M.; Hosono, H. *J. Ceram. Soc. Jpn.* **2005**, 113, 10.
- (11) Brechtel, E.; Cordier, G.; Schaefer, H. *Z. Naturforsch., B: Anorg. Chem., Org. Chem.* **1979**, 34, 777.
- (12) Enjalran, M.; Scalettar, R. T.; Kauzlarich, S. M. *Phys. Rev. B* **2000**, 61, 14570.
- (13) Ozawa, T. C.; Kauzlarich, S. M.; Bieringer, M.; Wiebe, C. R.; Greedan, J. E.; Gardner, J. S. *Chem. Mater.* **2001**, 13, 973.
- (14) Zhu, W. J.; Hor, P. H. *J. Solid State Chem.* **1997**, 130, 319.
- (15) Zhu, W. J.; Hor, P. H.; Jacobson, A. J.; Crisci, G.; Albright, T. A.; Wang, S. -H.; Vogt, T. J. *Am. Chem. Soc.* **1997**, 119, 12398.
- (16) Otschi, K.; Origino, H.; Shimoyama, J.; Kishio, K. *J. Low Temp. Phys.* **1999**, 117, 729.
- (17) Adamson, P.; Hadermann, J.; Smura, C. F.; Rutt, O. J.; Hyett, G.; Free, D. G.; Clarke, S. J. *Chem. Mater.* **2012**, 24, 2802.

- (18) Smura, C. F.; Parker, D. R.; Zbiri, M.; Johnson, M. R.; Gál, Z. A.; Clarke, S. J. *J. Am. Chem. Soc.* **2011**, 133, 2691.
- (19) Jin, S. F.; Chen, X. L.; Guo, J. G.; Lei, M.; Lin, J. J.; Xi, J. G.; Wang, W. J.; Wang, W. Y. *Inorg. Chem.* **2012**, 51, 10185.
- (20) Tiedje, O.; Krasovskii, E. E.; Schattke, W. *Phys. Rev. B* **2003**, 67, 134105.
- (21) Krishnapriyan, A.; Barton, P. T.; Miao, M.; Seshadri, R. *arXiv*: 1309.3041v1.
- (22) Hiramatsu, H.; Yanagi, H.; Kamiya, T.; Ueda, K.; Hirano, M.; Hosono, H. *Chem. Mater.* **2008**, 20, 326-334.
- (23) Yanagi, H.; Tate, J.; Park, S.; Park, C. -H.; Keszler, D. A.; Hirano, M.; Hosono, H. *J. Appl. Phys.* **2006**, 100, 083705.
- (24) Ueda, K.; Takafuji, K.; Yanagi, H.; Kamiya, T.; Hosono, H.; Hiramatsu, H.; Hirano, M.; Hamada, N. *J. Appl. Phys.* **2007**, 102, 113714.
- (25) Kim, G. C.; Cheon, M.; Park, I. S.; Ahmad, D.; Kim, Y. C. *arXiv*:1105.5868v1.
- (26) Liu, M. -L.; Wu, L. -B.; Huang, F. -Q.; Chen, L. -D.; Chen, I. -W. *J. Appl. Phys.* **2007**, 102, 116108.
- (27) Scanlon, D. O.; Watson, G. W. *Chem. Mater.* **2009**, 21, 5435.
- (28) Vajenine, G. V.; Hoffmann, R. *Inorg. Chem.* **1996**, 35, 451.
- (29) Takano, Y.; Yahagi, K.; Sekizawa, K. *Physica B* **1995**, 206, 764.
- (30) Ueda, K.; Hirose, S.; Kawazoe, H.; Hosono, H. *Chem. Mater.* **2001**, 13, 1880.
- (31) Evans, J. S. O.; Brogden, E. B.; Thompson, A. L.; Cordiner, R. L. *Chem. Commun.* **2002**, 912.

- (32) Hunter B. Rietica: A Visual Rietveld Program. International Union of Crystallography Commission on Powder Diffraction Newsletter No. 20, Summer, 1998. <http://www.rietica.org>.
- (33) Perdew, J. P.; Burke, K.; Ernzerhof, M. *Phys. Rev. Lett.* **1996**, 77, 3865.
- (34) Giannozzi, P. et al. *J. Phys.: Condens. Matter* **2009**, 21, 395502.
- (35) Garrity, K. F.; Bennett, J. W.; Rabe K. M.; Vanderbilt, D. *Comput. Mater. Sci.* **2014**, 81, 446.
- (36) Anisimov, V. I.; Solovyev, I. V.; Korotin, M. A.; Czyżyk, M. T.; Sawatzky, G. A. *Phys. Rev. B* **1993**, 48, 16929.
- (37) Liechtenstein, A. I.; Anisimov, V. I.; Zaanen, J. *Phys. Rev. B* **1995**, 52, R5467.
- (38) Monkhorst, H. J.; Pack, J. D. *Phys. Rev. B* **1976**, 13, 5188.
- (39) Barreteau, C.; Bèardan, D.; Amzallag, E.; Zhao, L. D.; Dragoë, N. *Chem. Mater.* **2012**, 24, 3168-3178.
- (40) Yang, H.; Liu, Y.; Zhuang, C.; Shi, J.; Yao, Y.; Massidda, S.; Monni, M.; Jia, Y.; Xi, X.; Li, Q.; Liu, Z. -K.; Feng, Q.; Wen, H. -H. *Phys. Rev. Lett.* **2008**, 101, 067001.
- (41) Cheng, P.; Yang, H.; Jia, Y.; Fang, L.; Zhu, X.; Mu, G.; Wen, H. H. *Phys. Rev. B* **2008**, 78, 134508.
- (42) Lu, F.; Zhao, J. Z.; Wang, W. H. *J. Phys.: Condens. Matter* **2012**, 24, 495501.